Development of a Real-Time Pulse Processing Algorithm for TES-Based X-Ray Microcalorimeters

Hui Tan, Wolfgang Hennig, William K. Warburton, W. Bertrand Doriese, and Caroline A. Kilbourne

***Abstract*—We report here a real-time pulse processing algorithm for superconducting transition-edge sensor (TES) based x-ray microcalorimeters. TES-based microcalorimeters offer ultra-high energy resolutions, but the small volume of each pixel requires that large arrays of identical microcalorimeter pixels be built to achieve sufficient detection efficiency. That in turn requires as much pulse processing as possible must be performed at the front end of readout electronics to avoid transferring large amounts of data to a host computer for post-processing. Therefore, a real-time pulse processing algorithm that not only can be implemented in the readout electronics but also achieve satisfactory energy resolutions is desired. We have developed an algorithm that can be easily implemented in hardware. We then tested the algorithm offline using several data sets acquired with an 8×8 Goddard TES x-ray calorimeter array and 2×16 NIST time-division SQUID multiplexer. We obtained an average energy resolution of close to 3.0 eV at 6 keV for the multiplexed pixels while preserving over 99% of the events in the data sets.**

***Index Terms*—Algorithm, microcalorimeters, optimal filter, real-time pulse processing, transition-edge sensors.**

I. Introduction

LARGE ARRAYS of superconducting transition-edge-sensor (TES) x-ray microcalorimeters have been developed in recent years for high-resolution x-ray spectroscopy. Multiplexed readout of these large arrays using superconducting quantum interference devices (SQUIDs) is generally required in order to decrease the heat loads and design complexity by reducing the number of wires running to the low temperature stages of the instrument [1]. Typically, multiplexed data stream from these arrays are first demultiplexed and then saved to computer hard drives in the form of triggered data records for later optimal filtering and analysis. It is clear that as microcalorimeter arrays become larger and larger, the amount of data that needs to be stored becomes prohibitively limited by available data bandwidth, especially for those spaceflight instruments where data has to be telemetered to the ground. Thus, it is hugely advantageous to process pulses right in the readout electronics in real time and to only transmit or store a limited data record for each event.

Manuscript received August 03, 2010; accepted September 20, 2010. Date of publication November 09, 2010; date of current version May 27, 2011. This work was supported in part by the U.S. Department of Energy under Grant DE-FG02-07ER84760.

H. Tan, W. Hennig, and W. K. Warburton are with XIA LLC, Hayward, CA 94544 USA (e-mail: htan@xia.com).

W. B. Doriese is with the National Institute of Standards and Technology, Boulder, CO 80305 USA (e-mail: doriese@boulder.nist.gov).

C. A. Kilbourne is with the National Aeronautics and Space Administration/Goddard Space Flight Center, Greenbelt, MD 20771 USA (e-mail: Caroline.A.Kilbourne@nasa.gov).

Digital Object Identifier 10.1109/TASC.2010.2082473

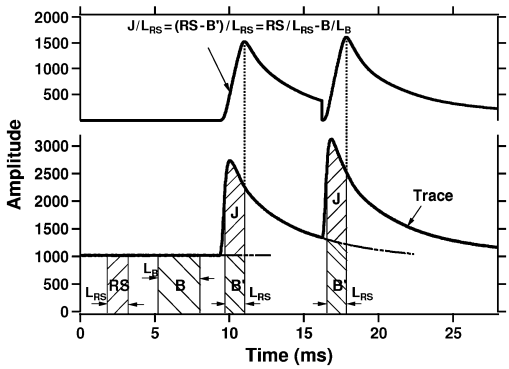

Fig. 1. Sketch illustrating XIA's filter algorithm for computing pulse height of microcalorimeter pulses.

Real-time microcalorimeter pulse processing based on optimal filtering [2] has been reported in various systems. Calorimeter Digital Processor (CDP) was developed for the Astro-E/Astro-E2 missions [3]. A full software implementation of the CDP, the Software Calorimeter Digital Processor (SCDP), has been deployed in the XRS/EBIT and the EBIT/ECS experiments at Lawrence Livermore National Laboratory [4]. A Digital Signal Processing System has also been developed for the X-ray Microcalorimeter onboard ASTRO-H [5]. Optimal-filter based data processing algorithms generally give excellent energy resolution, but are limited by the requirement for long record length and thus their throughput is generally low [6].

We have developed a digital pulse processing algorithm that gives similar energy resolution as optimal filter does but can achieve much higher throughput [7]–[9]. We have previously reported the filter algorithm for processing TES based gamma-ray microcalorimeter pulses. That filter achieved an energy resolution of 28.2 eV (FWHM) at 97 keV with an input count rate of ~3 cps, which was comparable to the energy resolution of 29.7 eV (FWHM) obtained by optimal filter. In this study, we adapted this filter towards high resolution TES X-ray microcalorimeter ^{55}Fe data acquired with an 8×8 Goddard TES X-ray calorimeter arrays and NIST time-division SQUID multiplexers.

II. Methods

A. A Brief Review of the Filter Algorithm

Fig. 1 illustrates the filter algorithm that XIA developed for processing microcalorimeter pulses. A running sum filter, RS, which is the summation of L_{RS} digitized trace data samples, is continuously updated upon the arrival of each new digitized trace data point. At the same time, a baseline filter, B, which is the summation of L_B digitized trace data samples, is also continuously updated and used as a measurement of the baseline

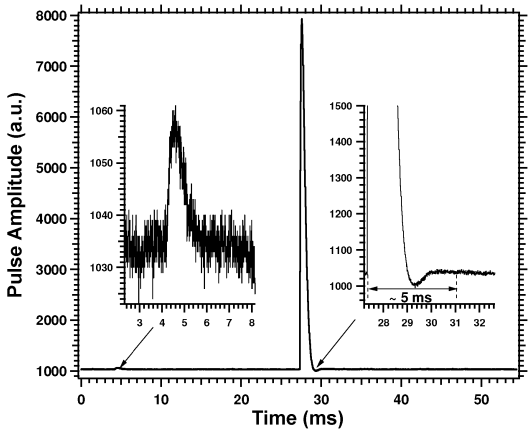

Fig. 2. Sample pulse shape for the Goddard/NIST TES X-ray microcalorimeter array.

of incoming traces. When a pulse is detected through a separate trigger filter, RS starts to measure contributions from both the baseline and the incident radiation event which generates the pulse. XIA's algorithm looks for the time when RS reaches its maximum. At that time, RS is stored, and B′, the contribution to the running sum from the baseline, is computed by scaling the baseline measurement immediately prior to the detection of the pulse with the running sum length $\mathrm{L_{RS}}$, i.e., $\mathrm{B'} = \mathrm{B} * \mathrm{L_{RS}}/\mathrm{L_B}$. The pulse height is then represented by the value of filter response $(\mathrm{RS} - \mathrm{B'})/\mathrm{L_{RS}}$, or $\mathrm{J}/\mathrm{L_{RS}}$, where J is the net area under the pulse when RS reaches its maximum as shown in the upper half of Fig. 1. To estimate B′ for a pulse sitting on the tail part of the previous pulse, e.g., the second pulse in Fig. 1, the shape of the preceding pulse's tail needs to be known in detail.

B. Pulse Shape for the Goddard/NIST TES X-Ray Microcalorimeter Array

Fig. 2 shows a sample pulse shape for the Goddard TES X-ray calorimeter array. This X-ray pulse is critically damped with a time constant of $\sim 280\ \mu\mathrm{s}$. We notice that there is an undershoot near the end of the pulse, as shown by the insert (right) in Fig. 2. This undershoot certainly complicates the computation of pulse height of a second pulse if it arrives near the undershoot region of this pulse, since we have to be able to characterize in detail this undershoot curve if we want to derive the pulse height of the second pulse accurately.

For this study, we chose to reject this type of pulses if they arrive too close to their preceding pulses for two reasons. First, the whole duration of one X-ray pulse is approximately 5 ms (measured from the start of the pulse to the time when the pulse returns to pre-trigger baseline level). A non-paralyzable detector with dead $\mathrm{time} = 5\,\mathrm{ms}$ would produce a maximum output count rate of ∼73 cps at an input count rate of 200 cps [10]. This might still be sufficient for most TES X-ray microcalorimeter applications. Moreover, the count rate for the data sets in this study is ∼2 counts/s. With dead $\mathrm{time} = 5\ \mathrm{ms}$, the pile-up rejection loss would be less than 1%. Second, due to the non-linearity of the microcalorimeter detectors, overlapping pulses produce non-uniform pulse heights even if same radiation energy is deposited in the detector. Removing these pulses from the energy resolution measurements will help us truly evaluate the performance of our filter algorithm.

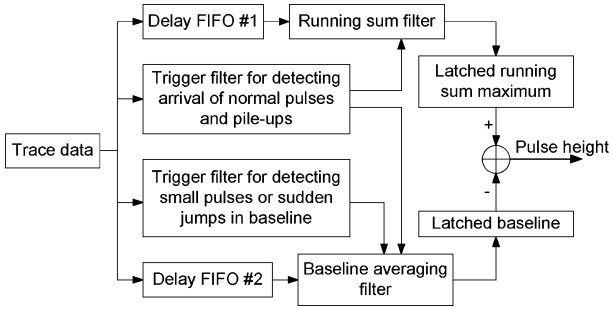

Fig. 3. Data flow in the implementation of XIA's microcalorimeter filter algorithms.

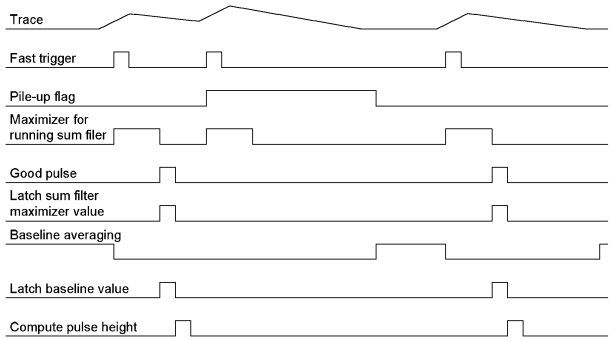

Fig. 4. Timing diagram for the implementation of XIA's microcalorimeter filter algorithm.

We also notice that there are occasional small "bumps" in the baseline of the sample pulse, as shown by the insert (left) in Fig. 2. They are too small to be detected by the regular trigger filter. If they are included in the baseline measurements, accuracy of the computed baseline will suffer and energy resolution will deteriorate. Thus, another trigger filter is needed to specifically detect and remove these small pulses from being included in baseline calculations.

C. Implementation of XIA's Microcalorimeter Filter Algorithms

Fig. 3 shows the data flow in the implementation of XIA's microcalorimeter filter algorithm. There are two trigger filters, one for detecting pulses and pile-ups, and the other for rejecting small pulses or sudden jumps when computing baseline. A running sum filter with length $\mathrm{L_{RS}}$ continuously updates its sum value as new trace data comes in. Similarly, a baseline averaging filter with length $\mathrm{L_B}$ continuously updates the baseline value except when there is a pulse present or the baseline experiences a large jump. The two delay FIFOs are used to compensate for the delays of the trigger filter response. If a pulse passes the pile-up rejection test, its running sum maximum and corresponding baseline value are latched and properly scaled, and the pulse height is computed by subtracting the baseline from the running sum maximum. The resulting pulse height is then binned into on-board histogram memory and can also be stored in list mode data memory for offline analysis, e.g., long term gain drifting correction, etc.

Fig. 4 illustrates a timing diagram for the implementation of XIA's microcalorimeter filter algorithm. At the top of the figure three pulses are shown, the second pulse being piled-up with the first pulse. The trigger filter detects the arrival of the pulses by

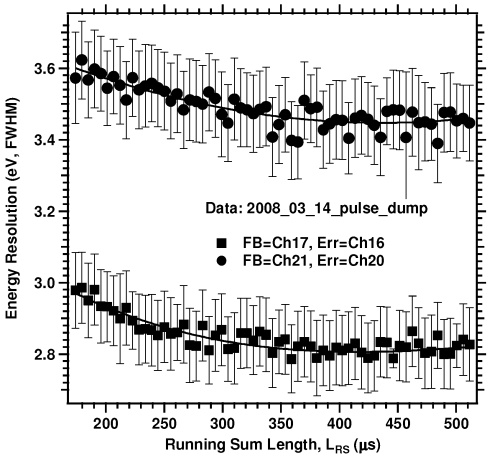

Fig. 5. Effect of running sum length for the XIA microcalorimeter filter on energy resolution.

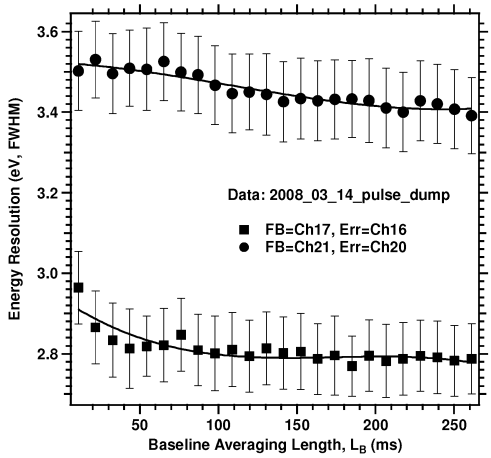

Fig. 6. Effect of baseline averaging length for the XIA microcalorimeter filter on energy resolution.

generating fast triggers. A pile-up flag is set to logic HIGH when the second pulse arrives but is cleared to logic LOW when no more pulse shows up within its pile-up inspection period $\mathrm{L_{PILE}}$. The maximizer for the running sum filter is activated at the arrival of each pulse and stops after the running sum length $\mathrm{L_{RS}}$ has expired. A pulse is considered to be "good" if the pile-up flag is logic LOW from the time when the pulse arrives to the time when the maximizer for the running sum filter stops. Therefore, the first and third pulses shown in Fig. 4 are good pulses and will have their pulse height values computed, whereas the second pulse is piled-up and will be rejected. Baseline averaging filter stops running during the pile-up inspection periods.

III. Results and Discussions

We have applied our microcalorimeter filter algorithm in offline mode to four sets of high resolution TES X-ray microcalorimeter $^{55}\mathrm{Fe}$ data recorded for Constellation-X/ IXO technology demonstrations in the spring of 2008. The data consist of streamed feedback and error data. The total size of these four data sets on hard disk is 564 GB.

A. Optimizing Running Sum Length

In order to achieve the best possible energy resolution with our microcalorimeter filters, we need to choose an optimal running sum length $\mathrm{L_{RS}}$. For TES microcalorimeter detectors, we believe a simple average of certain number of digitized samples around the peak of a TES pulse after subtracting its preceding baseline will produce an accurate measurement of such pulse. This of course implies that we are making an assumption that all TES pulses, or at least for those near the region of interested energies, have nearly identical pulse shape. This assumption in some sense is consistent with optimal filtering in which averaged pulse templates are used for processing microcalorimeter pulses.

Fig. 5 shows the scan of different running sum lengths. During the scan the pile-up rejection period $\mathrm{L_{PILE}}$ was set to 87.04 ms and the baseline averaging length $\mathrm{L_B}$ was set to 174.08 ms. Energy resolution for both channel pairs improves as the running sum length increases, which implies more averaging of trace data points suppresses further the noise associated with trace data. The energy resolution improves with increasing sum length until about 350 μs and changes little when sum length is near 400 to 450 μs. However, when the sum length increases further to over 500 μs, the energy resolution starts to get worse, which means additional averaging of trace data points is not helping the energy resolution anymore. Therefore, an optimal setting for the running sum length for these particular detector channels is 400 to 450 μs.

B. Optimizing Baseline Averaging Length

Another important parameter to optimize our microcalorimeter filter to obtain the best possible energy resolution is the baseline averaging length $\mathrm{L_B}$. Fig. 6 shows the scan of different baseline averaging lengths. During the scan the pile-up rejection period $\mathrm{L_{PILE}}$ was set to 4.08 ms and the running sum length $\mathrm{L_{RS}}$ was set to 435.2 μs. As expected, energy resolution for both channel pairs improves as the baseline averaging length increases since the more trace data points used for baseline averaging, the better on removing high frequency noise components in the baseline computation. However, after baseline averaging length reaches approximately 200 ms, the benefit of further baseline averaging to improve energy resolution is limited. When also taking into account the implementation of the baseline averaging filter in real hardware, the longer the filter, the more memory resources are needed. Therefore, a trade-off has to be made in order to achieve both good energy resolution and the ability to implement the baseline averaging filter in hardware. Fig. 6 demonstrates that the downside of reducing the baseline averaging length to $\sim$100 ms is still very small.

C. Optimizing Pile-Up Rejection Length

For our filter, minimal pile-up rejection length is defined as the duration from the time when a pulse arrives to the time the pulse fully decays back to its pre-trigger baseline level. However, much longer pile-up rejection length is not needed for our filter since the filter only need a small portion of trace near the pulse peak to derive its pulse height. In fact, longer pile-up rejection length will produce higher pile-up loss while benefiting energy resolution very little. This is reflected in Fig. 7, which shows the scan of different pile-up rejection lengths $\mathrm{L_{PILE}}$. During the scan the baseline averaging length $\mathrm{L_B}$ was

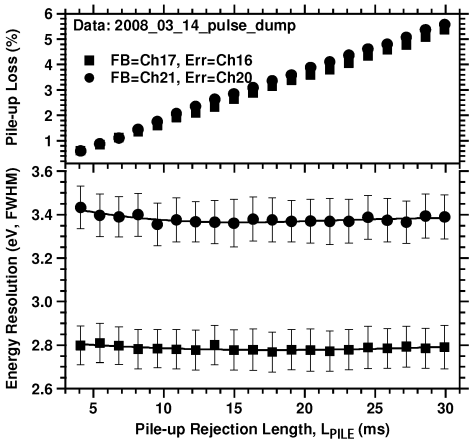

Fig. 7. Effect of pile-up rejection length for the XIA microcalorimeter filter on energy resolution.

set to 174.08 ms and the running sum length $\mathrm{L_{RS}}$ was set to 435.2 μs. For both channel pairs, pile-up loss rises steadily as $\mathrm{L_{PILE}}$ increases, but the energy resolution changes very little. Therefore, pile-up loss can be minimized when $\mathrm{L_{PILE}}$ is set to its minimally required value.

D. Correcting Gain Drift Over Time

A common issue among the four data sets is the gradual drift of the pulse baseline with time. The general trend is that the baseline increases with time. Correspondingly, pulse height decreases. We used the following method to correct this type of gain drift over time. First we computed the raw pulse height value for each event and stored the pulse height value and timestamp for each event in files. Then we plotted the pulse height values versus timestamps. On that plot, we identified the $\mathrm{K}\alpha_2$ peak of the Mn $\mathrm{K}\alpha$ doublet, and then fitted with a 4th order polynomial function the data points of the $\mathrm{K}\alpha_2$ peak's pulse height values versus the timestamps. Finally, we corrected the pulse height values for all events, i.e., events of both $\mathrm{K}\alpha_1$ and $\mathrm{K}\alpha_2$ peaks, using the fitted polynomial function.

E. Measured Energy Resolution and Event Acceptance Rate

Utilizing the optimal settings that were found above for the XIA filter, we measured the energy resolution and event acceptance rate for the four data sets. Here we define the event acceptance rate as the ratio of the number of accepted events by the filter to the total number of events in the data set.

In order to compare results of XIA filter to those of optimal filter, we used another four sets of data and analyzed them using optimal filter. We call these four sets of data "matching" data sets to the four data sets that were analyzed by the XIA filter since these "matching" data sets were acquired under the same detector conditions and around the same time as the four data sets analyzed by the XIA filter. However, these "matching" data sets are "records" instead of raw streamed data. Each record has 16384, 8192 and 6144 frames, or a length of 44.564 ms, 44.564 ms and 50.135 ms, for 2×4, 2×8 and 2×12 multiplexing, respectively.

Fig. 8 shows the comparison of energy resolution and acceptance rate between optimal filter and XIA filter for 2×4, 2×8 and 2×12 multiplexing, respectively. It also shows the predicted

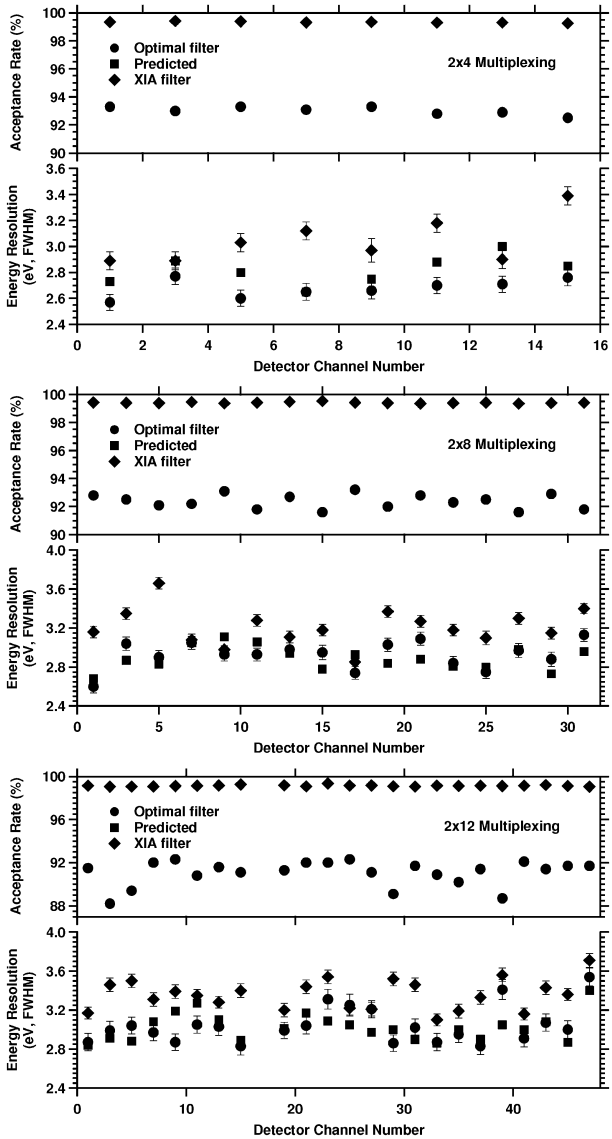

Fig. 8. Comparison of energy resolution and acceptance rate between optimal filter and XIA filter for 2 × 4, 2 × 8 and 2 × 12 multiplexing.

TABLE I
COMPARISON OF RESULTS BETWEEN XIA FILTER AND OPTIMAL FILTER

Multiplexing	Predicted Energy Resolution (eV, FWHM)	Measured Average Energy Resolution (eV, FWHM)		Average Record or Events Acceptance Rate (%)	
		Optimal Filter	XIA Filter	Optimal Filter	XIA Filter
2×4	2.82	2.68 ± 0.07	3.05 ± 0.18	93.0 ± 0.3	99.33 ± 0.05
2×8	2.89	2.93 ± 0.14	3.21 ± 0.19	92.4 ± 0.5	99.41 ± 0.05
2×12	3.02	3.04 ± 0.19	3.36 ± 0.15	91.1 ± 1.2	99.13 ± 0.07

energy resolution based on noise model. Optimal filter generally gives better energy resolution than XIA filter, or on average ∼0.3 eV better as shown in Table I. However, the XIA filter constantly gets much higher acceptance rate than optimal filter: over 99% for XIA filter versus ∼92% for optimal filter. At higher count rates, XIA filter is expected to achieve even higher output

count rates than optimal filter does, since XIA filter's dead time can be as short as the pulse duration.

REFERENCES

[1] C. A. Kilbourne, W. B. Doriese, S. R. Bandler, R. P. Brekosky, A. Brown, J. A. Chervenak, M. E. Eckart, F. M. Finkbeiner, G. C. Hilton, K. D. Irwin, N. Iyomoto, R. L. Kelley, F. S. Porter, C. D. Reintsema, S. J. Smith, and J. N. Ullom, "Multiplexed readout of uniform arrays of TES x-ray microcalorimeters suitable for Constellation-X," *Proc. SPIE*, vol. 7011, pp. 701104-1–701104-12, 2008.

[2] A. E. Symkowiak, R. L. Kelley, S. H. Moseley, and C. K. Stahle, "Signal processing for microcalorimeters," *J. Low Temp. Phys.*, vol. 93, no. 3/4, pp. 281–285, 1993.

[3] K. R. Boyce, M. D. Audley, R. G. Baker, J. J. Dumonthier, R. Fujimoto, K. C. Gendreau, Y. Ishisaki, R. L. Kelley, C. K. Stahle, A. E. Szymkowiak, and G. E. Winkert, "Design and performance of the Astro-E/XRS signal processing system," *Proc. SPIE*, vol. 3765, pp. 741–750, 1999.

[4] J. S. Adams, S. R. Bandler, L. E. Brown, K. R. Boyce, M. P. Chiao, W. B. Doriese, M. E. Eckart, G. C. Hilton, R. L. Kelley, C. A. Kilbourne, F. S. Porter, M. W. Rabin, S. J. Smith, D. D. Stewart, and J. N. Ullom, "Real-time data processing for X-ray spectroscopy," in *Proc. AIP Conf. (American Institute of Physics)*, B. Cabrera, A. Miller, and B. Young, Eds., 2009, vol. 1185, pp. 274–277.

[5] H. Seta, M. S. Tashiro, Y. Terada, Y. Shimoda, K. Onda, Y. Ishisaki, M. Tsujimoto, T. Hagihara, Y. Takei, K. Mitsuda, K. R. Boyce, and A. E. Szymkowiak, "Development of a digital signal processing system for the x-ray microcalorimeter onboard ASTRO-H," in *AIP Conf. Proc. (American Institute of Physics)*, B. Cabrera, A. Miller, and B. Young, Eds., 2009, vol. 1185, pp. 278–281.

[6] W. B. Doriese, J. S. Adams, G. C. Hilton, K. D. Irwin, C. A. Kilbourne, F. J. Schima, and J. N. Ullom, "Optimal filtering, record length, and count rate in transition-edge-sensor Microcalorimeters," in *AIP Conf. Proc. (American Institute of Physics)*, B. Cabrera, A. Miller, and B. Young, Eds., 2009, vol. 1185, pp. 450–453.

[7] H. Tan, D. Breus, W. Hennig, K. Sabourov, J. W. Collins, W. K. Warburton, W. Bertrand Doriese, J. N. Ullom, M. K. Bacrania, A. S. Hoover, and M. W. Rabin, "High rate pulse processing algorithms for microcalorimeters," in *AIP Conf. Proc. (American Institute of Physics)*, B. Cabrera, A. Miller, and B. Young, Eds., 2009, vol. 1185, pp. 294–297.

[8] H. Tan, D. Breus, W. Hennig, K. Sabourov, W. K. Warburton, W. B. Doriese, J. N. Ullom, M. K. Bacrania, A. S. Hoover, and M. W. Rabin, "High rate pulse processing algorithms for microcalorimeters," in *IEEE Nuclear Science Symp. Conf. Record*, 2008, pp. 1130–1133.

[9] H. Tan, J. W. Collins, W. Hennig, M. Walby, P. Grudberg, and W. K. Warburton, "Digital readout electronics for microcalorimeters," in *IEEE Nuclear Science Symp. Conf. Record*, 2009, pp. 341–344.

[10] G. F. Knoll, *Radiation Detection and Measurement*, 3rd ed. New York: Wiley, 2000.